Computation of Wind Tunnel Wall Effects in Ducted Rotor Experiments

A. L. Loeffler Jr.*
Grumman Aerospace Corporation, Bethpage, New York
and
J. S. Steinhoff†
University of Tennessee Space Institute, Tullahoma, Tennessee

Ducted propellers and turbines operating in a square closed wind tunnel test section are analyzed. A multiple image method is used to account for tunnel wall interference effects and a detailed method of singularities model is used for the ducted rotor. The size of the rotor wake is computed, taking into account the tunnel walls. Several ducted rotor model/wind tunnel dimension ratios are examined, ranging between 0.02 and 0.50. In addition, ducted rotor disk loading coefficients, C_{T_0}, between -30 and 0.89 are considered (the negative values correspond to the rotor acting as a propeller; the positive values indicate that the rotor is a turbine). Values of ideal propeller thrust are reduced by over 30% at the highest value of propeller disk loading ($C_{T_0} = -30$). The tunnel wall effect for a ducted turbine is less than for a ducted propeller and is opposite in direction. For the near-optimum condition $C_{T_0} = 0.89$, the ideal turbine power is increased by about 8% for the largest model/tunnel ratio considered.

Nomenclature

C_{P_i} = ideal thrust power coefficient for DAP (diffuser-augmented propeller) or ideal power coefficient for DAWT (diffuser-augmented wind turbine)
C_{T_0} = disk loading coefficient based on freestream dynamic head
D = dimension of wind tunnel test section
E = complete elliptic integral, Eq. (5)
K = complete elliptic integral, Eq. (4)
k_n = function of ring vortex coordinates and field point coordinates, Eq. (3)
N = the number of images along the side of a square image array
q = velocity in r direction
r = radial coordinate
r_p = ideal power augmentation ratio
R = diffuser radius at a particular value of z
S = the number of vortex rings used to represent the diffuser surface
T = total number of vortices used to represent both the diffuser and the wake
u = velocity in x direction
U_0 = freestream velocity, dimensional
v = velocity in y direction
w = velocity in z direction (axial direction)
x = lateral coordinate in plane perpendicular to mean flow
y = vertical coordinate in plane perpendicular to mean flow
z = coordinate in direction of mean flow
α = angle measured in counterclockwise direction relative to positive x axis. Refers to a direction line from centerline of actual DAP or DAWT, not to the images (see Fig. 2)
β = ratio of tunnel dimension D to maximum DAP or DAWT diameter
θ = half-angle of diffuser
ψ = stream function
Γ_n = vortex strength of the nth vortex ring

Subscripts
n = identifies vortex ring
$\mathfrak{L}$ = centerline
0 = quantity far upstream of diffuser
2 = quantity at diffuser inlet plane
4 = quantity at diffuser exit plane
5 = quantity far downstream of diffuser
(All quantities are dimensionless unless indicated otherwise.)

I. Introduction

DUCTED propulsion and power extraction systems are especially sensitive to wind tunnel wall interference effects because much of their effectiveness depends on streamtube shapes before and behind the duct. This sensitivity can be a major cost factor in aerodynamic development because practical model turbomachinery dictates a very large wind tunnel facility to ensure freedom from large interference errors. There is extensive literature[1-5] on wind tunnel corrections for flow around various closed bodies such as airfoils, but much less is known and available about corrections for open bodies such as ducted propellers. In a complete treatment, flow blockage effects due to both the ducted rotor body and its wake should be taken into account. In this paper, we discuss our use of the method of multiple images to predict closed wind tunnel interference effects which occur in testing models of two advanced ducted rotor concepts. These concepts are a diffuser-augmented propeller propulsion system (DAP) and a diffuser-augmented turbine wind energy conversion system (DAWT). Previously we analyzed the operation of these ducted rotors[6-8] in a flow of infinite extent. We chose the image method over other possible techniques, such as the panel method, because it is a natural extension of our earlier method of singularity work mentioned above. The present treatment is self-consistent in that the singularity strengths are determined exactly, taking into account the effects of the images.

Presented as Paper 84-0241 at the AIAA 22nd Aerospace Sciences Meeting, Reno, Nev., Jan. 9-12, 1984; received March 28, 1984; revision received Dec. 3, 1984.

*Staff Scientist, R&D Center. Member AIAA.
†Associate Professor, Department of Engineering Science.

II. Analysis

The basic flow model used for a conical DAP or DAWT is shown in Fig. 1. This scheme is suitable for the case of a model in an infinite medium. The diffuser cross-sectional radius at the upstream end where the propeller or turbine is located is R_2, while the exit radius is R_4. All length quantities have been nondimensionalized by the diffuser length so that the dimensionless overall length is unity. The effects of wind tunnel walls may be introduced into this flow model as indicated in Fig. 2. The center cell shows the cross section of the model located in a closed square test section wind tunnel at a particular longitudinal position, while the others are image cells outside the test section. The array shown here has $N=5$ images on a side, or 24 images altogether. It can be reasoned that the larger the number of images (N^2-1), the more nearly we will attain our goal of zero normal velocity at the tunnel walls. Numerical results will be shown later to verify this.

The origin of the (x, y) coordinates in Fig. 2 is at the lower left-hand side of the array, while z is measured down into the paper, with $z=0$ being the diffuser entrance (upstream) plane. The velocities in the x, y, and z directions are u, v, and w, respectively. All velocities have been made dimensionless using the uniform upstream tunnel velocity. The wind tunnel side-wall dimension is denoted by D.

The resultant velocity at any point within the wind tunnel (center cell) is the sum of the velocities induced by all the singularities, both those within the wind tunnel and those in the images. The computation time increases rapidly with the number of images so that it is important to use as small a value of N as possible. In our present analysis, the only singularities employed are vortex rings. Initially we consider the axisymmetric wind tunnel situation (the flowfield of Fig. 2 is not axisymmetric) simulated by a series of S vortex rings, all of which are located along the same diffuser centerline (Fig. 1). The radial coordinate relative to this line is r, while the axial coordinate is z. The velocities in the r and z direction are q and w, respectively, given by

$$q=\frac{1}{4\pi r^{3/2}}\sum_{n=1}^{T}\frac{\Gamma_n k_n(z-z_n)}{\sqrt{r_n}}\left\{K(k_n)-\left[1+\frac{k_n^2}{2(1-k_n^2)}\right]E(k_n)\right\} \tag{1}$$

$$w=\frac{1}{4\pi\sqrt{r}}\sum_{n=1}^{T}\frac{\Gamma_n k_n}{\sqrt{r_n}}\left\{K(k_n)-\left[1+\frac{[(r/r_n)-1]k_n^2}{2(r/r_n)(1-k_n^2)}\right]E(k_n)\right\} \tag{2}$$

where

$$k_n^2=\frac{4(r/r_n)}{[(z-z_n)/r_n]^2+[(r/r_n)+1)]^2} \tag{3}$$

and where Γ_n is the dimensionless strength of the nth vortex ring (see Nomenclature), r_n is the dimensionless nth vortex radius, and $K(k_n)$ and $E(k_n)$ are complete elliptic integrals defined as

$$K(k)=\int_0^{\pi/2}\frac{d\alpha}{\sqrt{1-k_n^2\sin^2\alpha}} \tag{4}$$

and

$$E(k_n)=\int_0^{\pi/2}\sqrt{1-k_n^2\sin^2\alpha}\,d\alpha \tag{5}$$

Another quantity of interest is the dimensionless induced stream function, namely,

$$\psi(z,r)=\frac{\sqrt{r}}{\pi}\sum_{n=1}^{T}\frac{\Gamma_n\sqrt{r_n}}{k_n}\left\{\left(1-\frac{k_n^2}{2}\right)K(k_n)-E(k_n)\right\} \tag{6}$$

As indicated before, Eqs. (1), (2), and (6) are valid for the axiysmmetric situation of coaxial vortices and therefore could describe quantities induced by the vortices in any single one of the cells, each with a total of T vortex rings shown in Fig. 2. What is desired, however, is to be able to compute the nonaxisymmetric values of u, v, and w at various field points within the central cell due to the vortex rings within the central cell, in addition to all those within the image cells. The total number of vortex rings that must be summed in Eqs. (1), (2), and (6) then is increased from T to N^2T. For this purpose, we can still use the foregoing equations with r being expressed in terms of x and y and the radial velocity q reinterpreted in terms of its u and v components. Thus

$$r=\sqrt{(x-x_n)^2+(y-y_n)^2}$$

where x_n, y_n are the coordinates of the nth vortex ring center and

$$u_n=\frac{(x-x_n)}{r}q,\quad v_n=\frac{(y-y_n)}{r}q$$

where u_n and v_n are the x and y velocities induced by the nth vortex at the position (x, y). To the sum of induced velocities at any field point (x, y) must be added the uniform upstream wind tunnel velocity U_0. In our dimensionless equations, this involves adding 1.0 to the w velocity and $r^2/2$ to ψ.

The foregoing are the basic equations required for our computations of wind tunnel interference effects. The method of solution here is similar to that used earlier.[6-8] That is, we require that the distribution of vorticity along the diffuser surface and the wake must satisfy the condition of zero normal velocity at the diffuser or wake surface and must also satisfy the Kutta condition that the velocity be bounded at the diffuser trailing edge. These requirements result in a system of simultaneous algebraic equations which couple to the wake

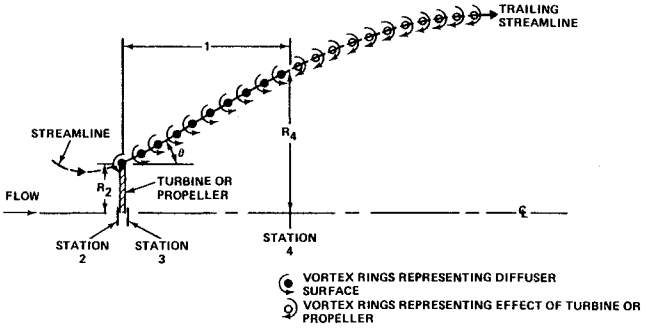

Fig. 1 Model using method of singularities.

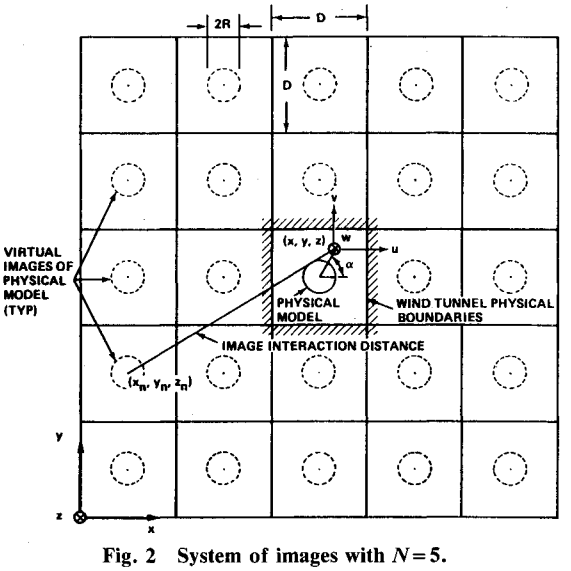

Fig. 2 System of images with $N=5$.

iterative solution to yield the vortex ring strengths. The expression for normal velocity at the diffuser or wake surface must include the image-induced velocities.

One difference between the previous axisymmetric analyses and the present non-axisymmetric one is that in the previous analyses we specified that the normal wall velocities be zero on circles located on the diffuser surface or wake midway between vortex rings. In this analysis, however, due to lack of axisymmetry, we cannot satisfy the boundary condition around the entire perimeter as we would like but only at particular azimuthal locations (two for each quadrant in the x-y plane for each value of z). In the present work, we chose $\alpha = \pi/8$ (see Fig. 2) as the locus of points at which the boundary condition (of zero normal velocity) was to be satisfied. This value of α was chosen as an average of 0 and $\pi/4$; the first of these represents a locus of points closest to an image, whereas the second is furthest from an image. We found that results for other values of α (e.g., 0 or $\pi/4$) do not differ appreciably from those of $\pi/8$. The present results are all for incompressible flow. There is no reason, however, why compressible flow could not be treated, for the linearized case, using the same general procedure presented here.

III. Results and Discussion

This paper provides a general method of computing closed wind tunnel interference effects for DAP and/or DAWT operation. We have chosen characteristic constant values for most parameters and have not attempted to cover the entire range of possible configurations of interest. Parameter values used herein for the computations are: $\theta = 40$ deg; $S = 10$; $R_2 = 1.0$; $T = 60$; $N = 1$, 3, and 5; and $\beta = 2$, 5, and 50. The diffuser geometry in all cases was an unslotted conical section, shown in Fig. 1. The Amdahl V6 computer was used for this work. For an image array with three images on a side, the CPU time required was about 46 min. For an image array with five images per side, the CPU time increased to about 141 min.

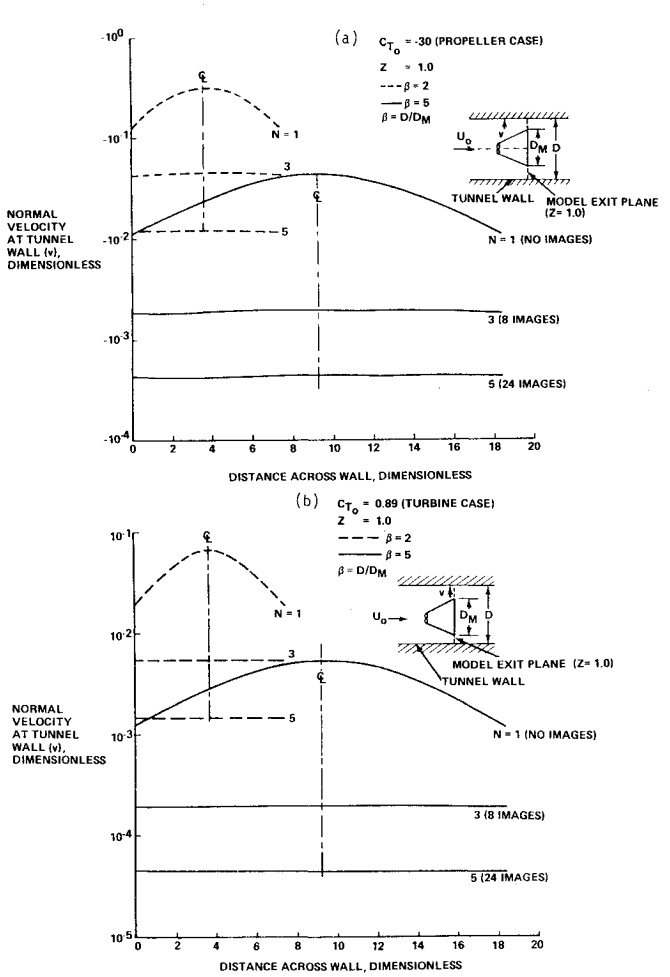

Fig. 3 Effect of image array size on normal velocity at horizontal tunnel wall.

In this paper the main purpose of using images is to represent a closed wind tunnel test, wherein the tunnel wall velocities are purely tangential. Thus, it seems desirable to ascertain the effectiveness of the images in reducing the normal velocities at the wall. Figure 3 shows the distribution of normal (nondimensional) velocity across the horizontal wind tunnel walls for three values of N and two values of β, the ratio of tunnel size to exit plane model diameter. Figure 3a is for a DAP with $C_{T_0} = -30$, while Fig. 3b is for a DAWT with $C_{T_0} = 0.89$. The normal wall velocities are seen to become negligibly small (less than 10% of their original value) as N increases from 1 to 5. The magnitudes of the normal velocities in Fig. 3a are much larger than those of Fig. 3b, but this is simply due to the larger absolute value of C_{T_0} in Fig. 3a. In general, the normal velocities are much higher (by at least an order of magnitude) for the case of $\beta = 2$ than for the corresponding curves for $\beta = 5$. This is to be expected since, for $\beta = 2$, the tunnel wall is much closer to the model than for $\beta = 5$ and the disturbance velocities would naturally be greater. The rapid decrease in normal flow component with increasing N, approaching the solid wall condition of a wind tunnel experiment even with the large model/test section ratio (small β of 2), is a gratifying result. It is interesting that the use of images not only reduces the magnitudes of the tunnel wall normal velocity but also yields an almost constant value of the velocity across the wall.

A more direct check of the convergence of our method than that used in Fig. 3 is to plot important flow parameters for the turbine or propeller, such as C_{P_i} for the turbine, against N. Unfortunately we have only three points for each such curve, namely, those points for $N = 1$, 3, and 5. Larger values of N were not run because of the much larger computation times. Due to the sparseness of points we have not presented plots but will simply state example results. Thus for the turbine case for $\beta = 2$ and $C_{T_0} = 0.89$, we obtained values of C_{P_i} (ideal power coefficient) of 2.780, 2.979, and 3.022 for values of N of 1, 3, and 5, respectively. These results appear to be converging.

In Figs. 4a-4d, we examine wind tunnel interference effects upon the diffuser exit plane axial velocity profile. An image array of five on a side ($N = 5$) was used to obtain these results. The profile in question is over a vertical traverse from the diffuser centerline to dimensionless distances of over eight. The wall for our 40-deg diffuser is located at a distance of 1.839. Each of the four plots is for a different value of disk loading coefficient C_{T_0}, namely, 0, 0.89, -1, and -30, respectively. The first plot (Fig. 4a) is the limiting case of zero disk loading for both a DAP and a DAWT. The second (Fig. 4b) represents a heavily loaded DAWT. The last two (Figs. 4c and 4d) are representative of a ducted propeller, lightly and heavily loaded, respectively. Each of the four plots contains curves for $\beta = 2$, 5, and 50. The parameter β is a measure for the ratio of tunnel size to model size. Large values of β indicate an approach to the infinite flow case, whereas small values of β mean that the tunnel size does not greatly exceed the model size. Wind tunnel interference effects would be expected to become appreciable for small enough β. An examination of Fig. 4 shows that the velocity profiles for $\beta = 5$ and 50 do not differ appreciably. Since $\beta = 50$ might be expected to approximate closely the infinite flow case where wind tunnel interference effects are negligible, we interpret the foregoing observation to indicate that interference effects are also small for $\beta = 5$. For $\beta = 2$, however, interference effects are appreciable, especially for the heavily loaded DAP case of Fig. 4d, where changes of velocity magnitude of over 20% occur near the diffuser centerline. The zero disk loading case in Fig. 4a shows very small tunnel interference effects.

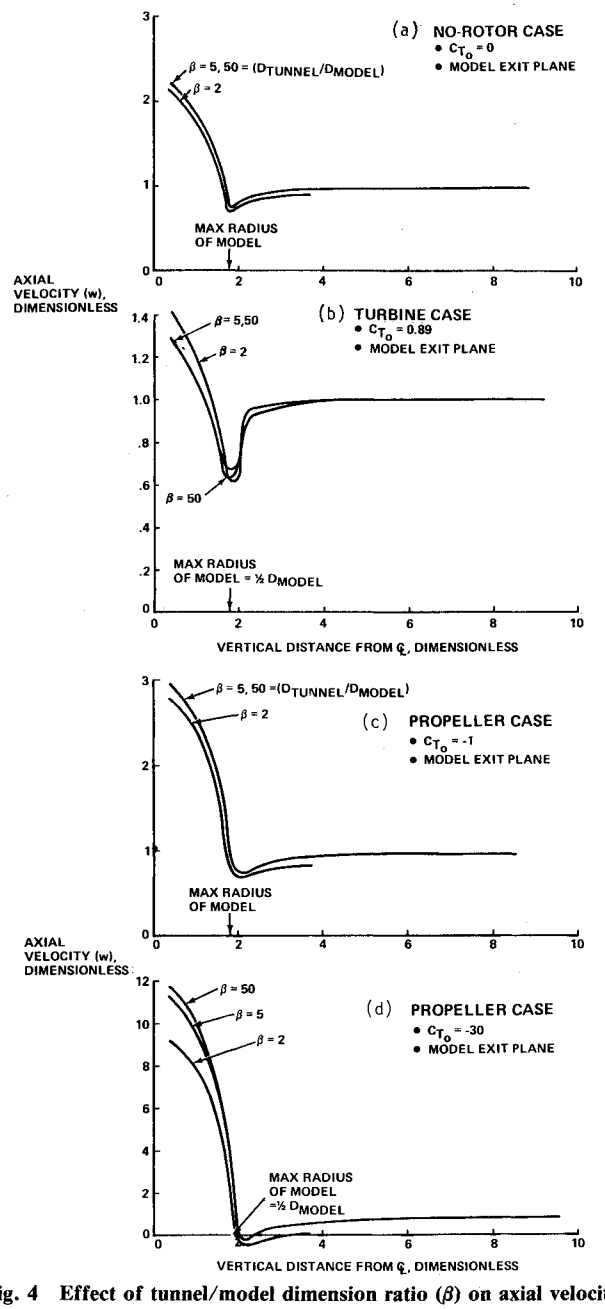

Fig. 4 Effect of tunnel/model dimension ratio (β) on axial velocity profile.

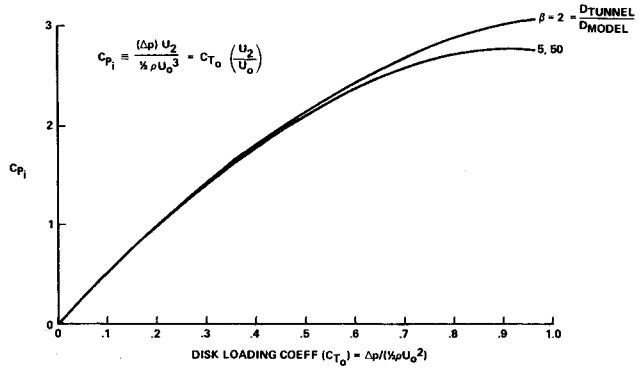

Fig. 5 Ideal turbine power coefficient vs C_{T_0} for three tunnel/model dimension ratios (β).

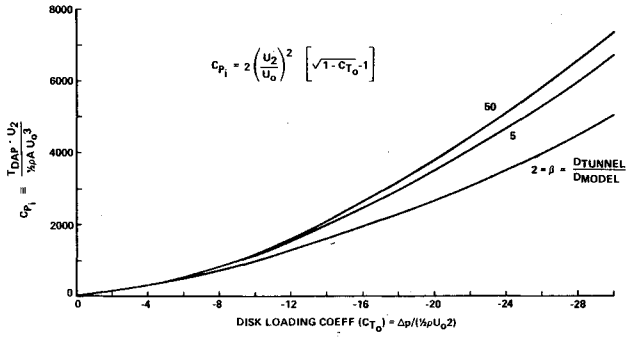

Fig. 6 Ideal propeller power coefficient vs C_{T_0} for three tunnel/model dimension ratios (β).

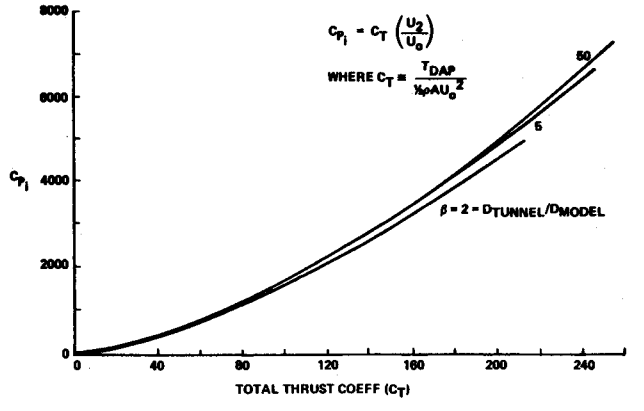

Fig. 7 Ideal propeller power coefficient vs total thrust coefficient for three tunnel/model dimension ratios (β).

Physically we might expect that a heavily loaded DAP operating in a relatively small tunnel would have less throughflow than for the case in a larger tunnel, since the volume of exterior flow to draw upon is limited by the tunnel walls. Figure 4d shows this to be true. Somewhat opposite reasoning holds for the case of a heavily loaded DAWT in a small tunnel; here the tunnel walls inhibit the tendency of the fluid to avoid the DAWT by flowing around it, and therefore more must flow through it. Figure 4b confirms this reasoning.

In Fig. 5 the ideal power coefficient C_{P_i} is plotted for a DAWT against disk loading coefficient C_{T_0} for the same three values of β of 50, 5, and 2. C_{P_i} is the maximum possible power producible by the DAWT made dimensionless with the freestream velocity and the density. The results for β of 5 and 50 indicate negligible wall interference, but for $\beta = 2$, C_{P_i} is increased by about 10% at the highest value of C_{T_0}. This observation is consistent with Fig. 4d, which shows an increase in flow through the DAWT for $\beta = 2$ due to tunnel wall interference effects. For small enough values of C_{T_0} (between 0 and -6) the tunnel effects on C_{P_i} disappear; this might have been anticipated since the wake distortion of the tunnel flowfield becomes less important at low disk loading coefficients.

The equations used in obtaining Figs. 5-9 are written on the figures and are easily derived from one-dimensional mass continuity and momentum considerations and from the definitions of the quantities involved.[8]

Figure 6 is similar to Fig. 5 but is for a DAP instead of a DAWT. At the large value of C_{T_0} considered here, there is some wall effect, even for $\beta = 5$ (maximum of 8.5%), but there is much more for $\beta = 2$ (maximum of 32%). As we would expect from Fig. 4, the wall effect is in the opposite direction from that in Fig. 5, namely, C_{P_i} is decreased rather than increased. Again, as in Fig. 5, the wall interference effects become negligible for small disk loading coefficients, as evidenced by the collapse of the curves into one curve.

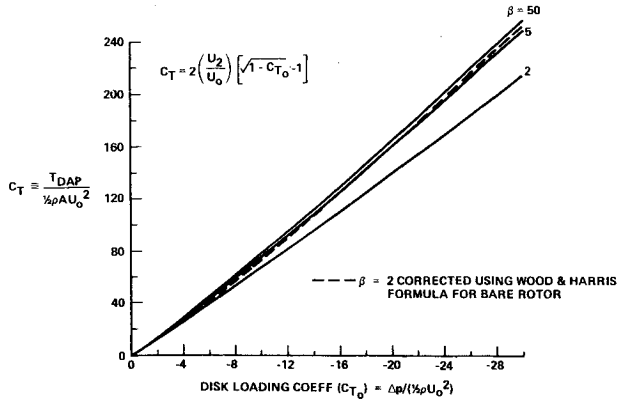

Fig. 8 Propeller thrust coefficient vs C_{T_0} for three tunnel/model dimension ratios (β).

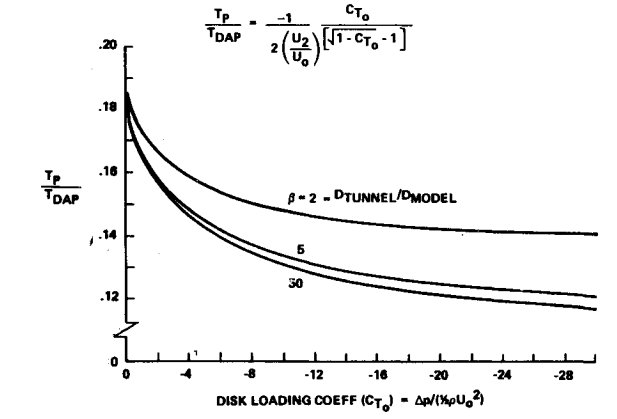

Fig. 9 Ratio of propeller thrust to total thrust vs C_{T_0} for three tunnel/model dimension ratios (β).

In Fig. 7, C_{P_i} is again the ordinate, but this time it is plotted against the total thrust coefficient C_T instead of the disk loading coefficient C_{T_0}. The spread in the curves is largely removed by this method of plotting. The explanation for this occurrence becomes evident from Fig. 8, where C_T is plotted against C_{T_0}. The results shown in Fig. 8 indicate that the magnitude of C_T for any given C_{T_0} is reduced by wall interference effects. This explains the compression of the three curves in Fig. 6 into the narrow band of Fig. 7. Figure 8 shows the results of applying an approximate wind tunnel correction formula.[1,9] Here we have applied the formula to correct our results for $\beta = 2$, and the corrected results agree reasonably well with those for infinite freestream flow (approximated by our $\beta = 50$ curve). This agreement is remarkable since the correction used was derived for a bare propeller and therefore neglects the large diffuser effect.

One important feature of a ducted propeller is the thrust force developed by the ducting in addition to the propeller thrust. This phenomenon has been discussed at length in Ref. 8. In wind tunnel testing the manner in which the thrust is proportioned between ducting and rotor might be expected to depend on the tunnel size relative to the model. Figure 9 demonstrates the existence and nature of this dependence. Here we have plotted the ratio of propeller thrust to the total DAP thrust (propeller plus diffuser thrust) against C_{T_0}, the disk loading coefficient. Decreasing the value of β (equivalent to increasing the tunnel wall interference effect) is seen to increase the propeller's share of the total thrust. This outcome is consistent with Fig. 4d, which showed that for $\beta = 2$ the flow rate within the diffuser is reduced, thereby reducing the diffuser thrust but not the propeller thrust since the latter does not depend directly on flow rate.

IV. Summary

A method of multiple images is used to predict closed wind tunnel interference effects which occur in testing both DAP and DAWT models. Our previously developed method of singularities representation of the flow around a model in an infinite freestream is used to describe both the physical model and the image flows. Propeller or turbine wake development, widely recognized as an important factor in tunnel interference effects, is accounted for in detail by an iterative method.

Use of a square image array with five images on a side (24 images total) gives good representation of the tunnel flow around a model, with normal velocities at the tunnel wall of approximately 1% or less of the tunnel mean velocity. The largest tunnel interference effects occur for the largest disk loading coefficients considered (i.e., $C_{T_0} = -30$ for DAPs and $C_{T_0} = 0.89$ for DAWTs). For diffuser-augmented propellers the tunnel interference effects are such as to reduce the mean flow through the propeller and thus to also reduce the ideal thrust power. For diffuser-augmented wind turbines the tunnel effects increase the flow through the turbine and thereby increase the ideal turbine power. An approximate wind tunnel correction formula originally derived by Wood and Harris for a bare propeller is shown to give good results even when a diffuser is also present.

References

[1]Glauert, H., "Wind Tunnel Interference on Wings, Bodies and Airscrews," Aeronautical Research Committee, R&M No. 1566, Sept. 1933.

[2]Allen, H. J. and Vincenti, W. G., "Wall interference in a Two-Dimensional-Flow Wind Tunnel, with Consideration of the Effect of Compressibility," NACA Report 782, 1944.

[3]Fackrell, J. E., Blockage Effects on Two-Dimensional Bluff Body Flow," *Aeronautical Quarterly*, Nov. 1975, pp. 243-253.

[4]Farell, C., Carrasquel, S., Guven, O. and Patel, V. C., "Effect of Wind-Tunnel Walls on the Flow Past Circular Cylinders and Cooling Tower Models," *Journal of Fluids Engineering, Transactions of the ASME*, Sept. 1977, pp. 470-479.

[5]Modi, V. J. and El-Sherbiny, S. E., "A Free-Streamline Model for Bluff Bodies in Confined Flow," *Journal of Fluids Engineering, Transactions of the ASME*, Sept. 1977, pp. 585-592.

[6]Loeffler, A. L. Jr. and Vanderbilt, D., "Inviscid Flow Through Wide-Angle Diffuser with Actuator Disk," *AIAA Journal*, Vol. 16, No. 10, Oct. 1978, pp. 1111-1112; see also Grumman Research Department Report RE-541, May 1977.

[7]Loeffler, A. L. Jr., "Flow Field Analysis and Performance of Wind Turbines Employing Slotted Diffusers," *Journal of Solar Energy Engineering*, Vol. 103, Feb. 1981, pp. 17-22; also Grumman Research Department Report RE-595, March 1980.

[8]Loeffler, A. L. Jr. and Foreman, K. M., "Analysis of a Diffuser Augmented Propeller," Grumman R&D Center Report RE-648, Oct. 1982.

[9]Wood and Harris, "Some Notes on the Theory of an Airscrew Working in a Wind Channel," R&M, No. 662, 1920.